NASA Technical Memorandum 100203

A Detailed Description of the Uncertainty Analysis for High Area Ratio Rocket Nozzle Tests at the NASA Lewis Research Center

Kenneth J. Davidian
Lewis Research Center
Cleveland, Ohio

Ronald H. Dieck
Pratt & Whitney
West Palm Beach, Florida

and

Isaac Chuang
Lewis Research Center
Cleveland, Ohio

Prepared for the
24th JANNAF Combustion Meeting
Monterey, California, October 5-9, 1987

NASA

A Detailed Description of the Uncertainty Analysis for High Area Ratio Rocket Nozzle Tests at the NASA Lewis Research Center

Kenneth J. Davidian
NASA Lewis Research Center
Cleveland, Ohio

Ronald H. Dieck
Pratt & Whitney
West Palm Beach, Florida

Isaac Chuang*
NASA Lewis Research Center
Cleveland, Ohio

ABSTRACT

A preliminary uncertainty analysis has been performed for the High Area Ratio Rocket Nozzle test program which took place at the altitude test capsule of the Rocket Engine Test Faciltiy at the NASA Lewis Research Center. Results from the study establish the uncertainty of measured and calculated parameters required for the calculation of rocket engine specific impulse. A generalized description of the uncertainty methodology employed is provided. Specific equations used and a detailed description of the analysis are presented. Verification of the uncertainty analysis model was performed by comparison with results from the experimental program's data reduction code. Final results include an uncertainty for specific impulse of 1.30%. Largest contributors to this uncertainty were calibration errors from the test capsule pressure and thrust measurement devices.

INTRODUCTION

The specific impulse of a rocket engine is one of the most important performance parameters. Results of mission analyses and vehicle sizing studies are dependent on the accuracy of the value used for an engine's specific impulse. Computer predictions of specific impulse for engines with high area ratio nozzles (a domain for which the codes were not designed) can be compared with experimentally measured values to verify the analytical output. To insure meaningful correlation between computer and test results, the specific impulse should be measured as accurately as possible. This report details an uncertainty analysis performed on data from rocket engine tests at the NASA Lewis Research Center.

A measurement uncertainty methodology for chemical rocket engines has been establish by JANNAF (Joint Army Navy NASA Air Force), formerly the Interagency Chemical Rocket Propulsion Group (ICRPG) (ref. 1). A goal of 0.25% on specific impulse uncertainty has been suggested and has been the topic of recent study (ref. 2).

The objective of this study was to determine the uncertainty on the calculated value of specific impulse from measurements taken during the High Area Ratio Nozzle test program. Uncertainties

*Summer Student from Massechusetts Institute of Technology

for measured parameters used in the calculation of specific impulse are given along with thoses for other measured and calculated parameters of interest.

The following assumptions were made in the analysis:

1. The experiment for which the uncertainty analysis was performed consists of carefully controlled measurement processes and calibration corrections for all instrumentation were perfectly carried out. This eliminated large bias errors of known magnitude. Small bias errors were assumed to be zero. In reality, the bias errors of measuring devices are not zero, although they generally are very small. An example of a small bias of unknown magnitude would be the reported uncertainty of a transducer which was calibrated by the National Bureau of Standards and which was incorporated into the test set-up. The level of uncertainty is unknown (only the range is known) and is fixed. Hence, it contributes to the experimental uncertainty as a bias error.

2. All data reduction errors were zero. For this experiment, this assumption is reasonable since the computer truncation errors and high order curve fit errors are negligible.

Although a general expectation of uncertainty may be obtained from an uncertainty analysis, many uncertainty analyses are tailored specifically for a given test, a given set of instruments, or a given set of data reduction equations. For this study, the experiment being analyzed is a rocket engine which employs gaseous hydrogen and gaseous oxygen as its fuel and oxidizer. The experiment was run at the NASA Lewis Research Center's Rocket Engine Test Facility (RETF) inside a low pressure capsule to simulate altitude conditions.

GENERALIZED DESCRIPTION OF THE UNCERTAINTY METHODOLOGY

The uncertainty methodology is described for different applications in references 1 and 3 through 27 and is described in detail in references 3 and 19. Only the basic principles will be discussed here for clarity.

Measurement Error

All measurements have uncertainties which are associated with experimental errors. These are the differences between the measured and an accepted standard true value. The total error of a measurement is usually expressed in terms of two components: a random (precision) error and a fixed or systematic (bias) error.

Precision Error

The distribution of a set of data points caused by random error are characterized by the standard deviation. The precision error range is defined to be twice the standard deviation for a large sample of data (more than 30 data points) and includes approximately 95% of the total scatter of measurements (ref. 27).The precision index of the data, S_X, approximates the true value of standard deviation and is defined by:

$$S_X = \sqrt{\frac{\sum_{i=1}^{N}(X_i - \overline{X})^2}{N-1}} \tag{1}$$

where N is the number of data points averaged, $\overline{X}$ is the average of the N data points, and X_i is the i^{th} individual data point.

The precision index of the average of a set of measurements is always less than that of an individual measurement. The precision index of an average, $S_{\overline{X}}$, is defined as:

$$S_{\overline{X}} = \sqrt{\frac{\sum_{i=1}^{N}(X_i - \overline{X})^2}{N(N-1)}} \tag{2}$$

It should be noted that the precision index, S_X, may also be estimated by assessing the variability of data about a curve fit. This variability, called the Standard Estimate of Error (SEE) is calculated as:

$$SEE = \sqrt{\frac{\sum_{i=1}^{N}(y_i - y_{i,c})^2}{N-C}} \tag{3}$$

where y_i is the i^{th} y value, $y_{i,c}$ is the equivalent y_i calculated from the curve fit at X_i, N is the number of data points, and C is the number of constants in the curve fit.

If many estimates of the same precision index are available, a better estimate of S_X may be had by "pooling" the estimates as follows:

$$S_p = \sqrt{\frac{\sum_{i=1}^{N}\nu_i S_i^2}{\sum_{i=1}^{N}\nu_i}} \tag{4}$$

where S_p is the pooled precision index and ν_i is the degrees of freedom of the i^{th} estimate of S_X.

Bias Error

Bias error is a systematic error which remains constant during a given test. Thus, in repeated measurements of a given variable, each measurement has the same bias. Note that it is assumed that the uncertainty analysis is applied to a carefully controlled measurement process within which all known calibration corrections have been made. If these calibrations were perfect, there would be no bias error. However, there always remains some systematic error of unknown magnitude. This bias error remaining must be estimated. If there is no statistical equation with which to determine a value, the estimate of the bias limit, B, must be based on judgement. Reference 27 provides several methods for estimating this bias error.

Combining Errors

In describing the precision and accuracy of a measurement, there is a need for a single value to quantitatively categorize the data adequacy. In obtaining this value, it is useful to group the error source.

Sources of error can be divided into three categories: calibration errors, data acquisition errors, and data reduction errors. Each of these sources of error have components of bias and precision error.

To obtain the bias of a given parameter (such as temperature or pressure), the root sum square (RSS) method is used to combine the bias limits from numerous (N) elemental sources of error. Thus

$$B = \sqrt{B_1^2 + B_2^2 + \cdots + B_N^2} \tag{5}$$

where B is the bias limit of a parameter and B_i is the bias limit for the i^{th} elemental error source. Similarly,

$$S = \sqrt{S_1^2 + S_2^2 + \cdots + S_N^2} \tag{6}$$

where S is the precision index of a parameter and S_i is the precision index for the i^{th} elemental error source.

For most experimental decisions, a single number is needed to express a reasonable limit of error for a given parameter. A model for combining the bias and precision errors, therefore, must be adopted which will yield the interval $X \pm U$, where U is the measurement uncertainty. U is a band within which the true value of the parameter is expected to lie, for some specified coverage. While no rigorous confidence level can be associated with the uncertainty, coverages analogous to the 95% and 99% confidence levels can be given for the two recommended uncertainty models (ref. 27). Thus one uses

$$U_{99} = B + t_{95}S \tag{7}$$

for approximately 99% coverage and

$$U_{95} = \sqrt{B^2 + (t_{95}S)^2} \tag{8}$$

for approximately 95% coverage. U_{99} and U_{95} are also referred to as U_{ADD} and U_{RSS}, respectively.

The Student's t value , t_{95}, is a function of the degrees of freedom used in calculating S_X. For large samples, (i.e., $N \geq 30$), t_{95} is set equal to 2. Table I gives the values for t_{95} for different values of degrees of freedom. Otherwise the Welch-Satterthwaite formula is used to provide the degrees of freedom, ν, according to

$$\nu = \frac{(\sum_{i=1}^{N} S_i^2)^2}{\sum_{i=1}^{N} \frac{S_i^4}{\nu_i}} \tag{9}$$

where S_i represents the precision indices of the various error sources involved, and ν_i represents the degrees of freedom associated with those error sources.

Uncertainty of a Result

Errors in measurements of various parameters (P) are often propagated into a derived result (r) through the functional relationship between the result and those parameters. The existence of such a relationship requires the use of influence coefficients (θ_i) which are used to obtain the error propagated to the result because of a unit error in the parameter. Thus if

$$r = f(P_1, P_2, P_3, \ldots, P_N) \tag{10}$$

where N is the number of parameters involved, and r is the computed result, then the influence coefficients are:

$$\theta_i = \frac{\partial r}{\partial P_i} \tag{11}$$

It is important to note that, as in all uncertainty analyses, the bias and precision errors of the parameters are kept separate until the last step, computing the uncertainty of a result.

The precision index of a result, S_r, is given by

$$S_r = \sqrt{\sum_{i=1}^{N} (\theta_i S_{P_i})^2} \tag{12}$$

Similarly, the bias limit of a result, B_r, is given by

$$B_r = \sqrt{\sum_{i=1}^{N} (\theta_i B_{P_i})^2} \tag{13}$$

The uncertainty of a result is given by either of the two uncertainty models shown above. The Student's t value is defined as before.

The Welch-Satterthwaite formula is used to provide ν_r and is slightly more complex. It's formula is

$$\nu_r = \frac{(\sum_{i=1}^{N}(\theta_i S_{P_i})^2)^2}{\sum_{i=1}^{N}\frac{(\theta_i S_{P_i})^4}{\nu_i}} \tag{14}$$

Note the influence coefficients convert each S_{P_i} into units identical to those of the result, a necessary step for combination.

UNCERTAINTY ANALYSIS DESCRIPTION

Facility Description

The altitude test chamber in the RETF includes a test capsule, diffuser, spray cooler, ejectors, liquid drain lines, and the water detention tank. The exhaust gases of the rocket engine aid in altitude pumping by passing through a second throat diffuser before exhausting into the spray cooler. Approximately half of the exhaust gases are condensed to a liquid and pass down the drains to the water detention tank. Ejectors, driven by gaseous nitrogen, pump the remaining exhaust gases through two short stacks to the atmosphere.

The engine instrumentation system is displayed in Fig. 1. Propellant flow rates are determined using calibrated venturis. Temperatures are measured using Chromel-Constantan thermocouples. A thermocouple type vacuum gauge is used to measure the vacuum reference pressure while the remaining pressures are measured by strain-gauge bridge type pressure transducers. Absolute and differential pressure transducers are used. The thrust stand is capable of measuring thrust levels to 13.3 KN (3000 lb_f) and was designed to have a random error of less than $\pm$ 0.1% of full scale. For more information on the facility, see reference 28.

Instrumentation in the facility's data acquisition system provides analog signals that are recorded and converted to a digital signal by an automatic data digitizer at a rate of 50 readings per second per parameter and sent to an IBM 370 computer. The computer averages the values in groups of five to provide data output at $\frac{1}{10}$ second intervals.

Site thrust, the force actually acting on the test stand, was measured by a triad of load cells in a parallel configuration to account for a thrust vector which is not perfectly aligned with the rocket engine's centerline axis. Similarly, other transducers may be shown in Fig. 1 as one device when, in fact, there may be more than one instrument recording data at that location. In these cases, the redundancy was to identify faulty transducers should one fail.

Upstream of the subsonic venturi, propellant line pressure and temperature were recorded. Just upstream of the injector, each propellant's pressure and temperature was again measured. Pressure transducers were located in the combustion chamber and differential transducers between the injector and chamber pressure transducers to allow for direct measurement of injector pressure drop. Redundant measurements of injector pressure drop were also obtained by subtracting the chamber pressure from the injection pressure. Differential pressure transducers, referenced to a vacuum tank, were used to measure nozzle wall static pressure and capsule (ambient) pressure.

Equations Used to Reduce Data

Experimentally, only the measurements of site thrust, capsule pressure, propellant line pressure and temperature, and differential pressure from the propellant line to the venturi throat were required

to calculate the rocket engine's specific impulse. Data reduction equations used to compute specific impulse are described below.

Pressure at the venturi throat. Throat pressure of the hydrogen and oxygen subsonic venturi flow meters, p_{th}, was calculated by:

$$p_{th} = p_{line} - dp \tag{15}$$

where p_{line} is the static pressure measurement upstream of the venturi and dp is the differential pressure measurement from the p_{line} transducer to the venturi throat.

Line contraction ratio. Propellant line contraction ratio, β, was defined by:

$$\beta = \frac{d_{th}}{d_{line}} \tag{16}$$

where d_{th} is the venturi throat diameter and d_{line} is the propellant line diameter.

Thermodynamic properties. Using the measured values of fluid pressure and temperature upstream of the venturi throat, the enthalpy, density, and entropy of the propellants in the propellant lines were determined using the Gas Properties program (GASP) (ref. 29). By assuming isentropic flow to the venturi throat, the throat pressure, calculated using Eq. (15), and the propellant entropy values were input to GASP to determine the fluid temperature, density, and enthalpy at the venturi throat.

Velocity at the venturi throat. Velocity of each fluid at the venturi throat, V_{th}, was determined by:

$$V_{th} = \sqrt{\frac{K(h_{line} - h_{th})}{[1 - (\frac{\rho_{th}}{\rho_{line}})^2 \beta^4]}} \tag{17}$$

where K was a conversion constant equal to 50079.5 $[\frac{(ft/sec)^2}{BTU/lb_m}]$, h_{line} and h_{th} are the propellant line and venturi throat enthalpies, and ρ_{line} and ρ_{th} are the propellant line and venturi throat densities.

Propellant mass flow rate. Mass flow rates for each propellant, $\dot{m}$, were determined from:

$$\dot{m} = C_d \frac{\pi}{4} d_{th}^2 \rho_{th} V_{th} \tag{18}$$

where C_d is the venturi discharge coefficient. Discharge coefficient error was determined by independant calibration and its calibration incorporates any error in the determination of venturi throat diameter.

The set of equations presented to this point, with the exception of Eq. (16), were employed four times in the data reduction procedure, once for each of the two oxygen line differential pressure measurements and once for each of the two hydrogen line differential pressure measurements. Hence, two values of oxygen and hydrogen throat pressure, thermodynamic properties, venturi throat velocity, and mass flow rates were calculated. Both oxygen mass flow rates were combined to arrive at an average value of oxygen mass flow rate, and the same procedure was followed for the fuel mass flow rates.

Total mass flow rate. The total mass flow rate, $\dot{m}_{TOT}$, was simply the sum of the mass flow rates of each fluid, namely:

$$\dot{m}_{TOT} = \dot{m}_{ox} + \dot{m}_{fu} \tag{19}$$

Vacuum thrust. Since the site thrust, F_{site}, was measured in an imperfect vacuum, a correction was applied:

$$F_{vac} = F_{site} + p_{amb} A_{exit} \tag{20}$$

where F_{vac} is the vacuum thrust, p_{amb} is the ambient, or capsule, pressure and A_{exit} is the rocket nozzle exit area.

Vacuum specific impulse. The performance parameter, vacuum specific impulse, I_{sp}. This parameter was calculated by:

$$I_{sp} = \frac{F_{vac}}{\dot{m}_{TOT}} \tag{21}$$

Propagation of Errors

Errors which occur in measured parameters are propagated to the calculated parameters through the use of influence coefficients. Sixteen basic measurements, or primary parameters, were collected in this experiment. These parameters were the propellant line pressures, temperatures, and diameters, differential pressure from the line to the subsonic venturi throat, the venturi throat diameter, the nozzle exit area, the measured thrust, and the altitude capsule (ambient) pressure.

These quantities were used to calculate certain variables, secondary parameters, such as the geometric and thermodynamic quantities. In turn, these were used to calculate the tertiary, or performance, parameters. Influence coefficients for the tertiary parameters with respect to the secondary parameters were calculated. However, these were not used to propagate the errors from the secondary to the tertiary results. Chain rule applications were employed to arrive at the partial derivative of the tertiary parameter with respect to the primary parameters. Since the secondary parameters were often functions of the same primary parameters, the partial derivatives of tertiary to secondary parameters did not accurately describe the ultimate effects of primary parameters upon the tertiary quantities.

To validate the values of the partial derivatives which were used for the uncertainty analysis, inputs to the data reduction program used for the rocket engine tests were parametrically perturbed to determine the effect this would have on calculated specific impulse. The result was a value for the change of specific impulse with respect to a change of one of the primary parameters. By comparing output from the data reduction computer program with the partial derivates computed using the uncertainty analysis model, the validity of the influence coefficients, as well as the uncertainty model as a whole, was confirmed. An attempt was made to use the partial derivatives of tertiary to secondary parameters and calculate the effect of primary variables upon tertiary results through the error propagation equation, Eq. (12). Values for the influence coefficients did not match the data reduction program results, indicating the incorrectness of the attempt to calculate errors of tertiary parameters using intermediate (secondary) results. This mistake was basis for the author's previous work (ref. 30) but has been corrected for in this study.

For example, the propellant line density and enthalpy are calculated using the line temperature and pressure. Errors are propagated from the temperature and pressure measurements to these thermodynamic properties using influence coefficients. Later, the venturi throat velocity is calculated as a function of the propellant line enthalpy and density. Velocity error is a combination (in part) of the propellant line enthalpy and density errors, however, since both of these properties are functions of the same basic measurements (temperature and pressure), combination of errors at the thermodynamic properties level leads to a greatly inflated value of error for the venturi throat velocity value. Therefore, the influence of propellant line pressure and temperature on velocity at the venturi throat, as described by partial derivatives calculated using the chain rule, must be computed to insure that all variables are independent of each other.

Description of the Influence Coefficients

Influence coefficients are required in the uncertainty methodology to propagate errors in measured parameters to errors in calculated parameters. Wherever possible, the influence coefficients were derived by using partial differentiation on the data reduction equations. To calculate the influence

coefficients for the propellant line and venturi throat thermodynamic properties, a perturbation method was used. Where partial differentiation of a calculated parameter was taken with respect to another calculated parameter, the chain rule was applied to attain the partial derivative with respect to one of the measured parameters, i.e. line pressure, line temperature, and differential pressure. Calculations for all influence coefficients are described below.

Pressure at the venturi throat. Computation of these influence coefficients was accomplished easily:

$$\frac{\partial p_{th}}{\partial p_{line}} = 1 \tag{22}$$

$$\frac{\partial p_{th}}{\partial dp} = -1 \tag{23}$$

Absolute values of these coefficients are unity for both propellants. This results from the fact that there exists a one-to-one relationship between an error in line pressure or differential pressure to an error in calculated throat pressure. Units of these influence coefficients are *psia/psia*.

Line contraction ratio. The line contraction ratio influence coefficients were found to be:

$$\frac{\partial \beta}{\partial d_{th}} = \frac{1}{d_{line}} \tag{24}$$

$$\frac{\partial \beta}{\partial d_{line}} = -\frac{d_{th}}{d_{line}^2} \tag{25}$$

Although the propellant line diameters were the same for both propellants, the oxygen and hydrogen venturi throat diameters were different which resulted in slightly different values for the influence coefficient expressed by Eq. (25). Typical values are 0.62 $inches^{-1}$ for the value of Eq. (24) (both oxygen and hydrogen terms) and –0.16 $inches^{-1}$ and –0.17 $inches^{-1}$ for the value of Eq. (25), for the oxidizer and fuel lines, respectively.

Thermodynamic properties. Influence coefficients of each calculated property with respect to both input properties were computed by perturbing each input parameter by a small amount (typically 1%) and noting the effect that this change produced in the result. Tables II and III show typical values for each influence coefficient calculated in this manner.

Since the partial derivatives in Table III are taken with respect to calculated parameters, they need to be reduced via the chain rule to partial derivatives with respect to line pressure, line temperature, and differential pressure. Equations (26), (27), and (28) give the generalized expressions which express the errors in the venturi throat thermodynamic properties as a function of the measured quantities.

$$\frac{\partial \phi}{\partial p_{line}} = \frac{\partial \phi}{\partial p_{th}} \frac{\partial p_{th}}{\partial p_{line}} + \frac{\partial \phi}{\partial s_{line}} \frac{\partial s_{line}}{\partial p_{line}} \tag{26}$$

$$\frac{\partial \phi}{\partial dp} = \frac{\partial \phi}{\partial p_{th}} \frac{\partial p_{th}}{\partial dp} \tag{27}$$

$$\frac{\partial \phi}{\partial T_{line}} = \frac{\partial \phi}{\partial s_{line}} \frac{\partial s_{line}}{\partial T_{line}} \tag{28}$$

where ϕ, the generalized variable, represents venturi throat enthalpy, density, and temperature.

Velocity at the venturi throat. Expressions for the partial derivatives of the venturi throat propellant velocity, Eq. (17), are shown below.

$$\frac{\partial V_{th}}{\partial h_{line}} = \frac{\sqrt{K}}{2\sqrt{(h_{line} - h_{th})[1 - (\frac{\rho_{th}}{\rho_{line}})^2 \beta^4]}} \tag{29}$$

$$\frac{\partial V_{th}}{\partial h_{th}} = -\frac{\partial V_{th}}{\partial h_{line}} \tag{30}$$

$$\frac{\partial V_{th}}{\partial \rho_{line}} = -\frac{\rho_{th}^2}{\rho_{line}^3} \frac{V_{th}\beta^4}{[1-(\frac{\rho_{th}}{\rho_{line}})^2\beta^4]} \tag{31}$$

$$\frac{\partial V_{th}}{\partial \rho_{th}} = \frac{\rho_{th}}{\rho_{line}^2} \frac{V_{th}\beta^4}{[1-(\frac{\rho_{th}}{\rho_{line}})^2\beta^4]} \tag{32}$$

$$\frac{\partial V_{th}}{\partial \beta} = \left(\frac{\rho_{th}}{\rho_{line}}\right)^2 \frac{2V_{th}\beta^3}{[1-(\frac{\rho_{th}}{\rho_{line}})^2\beta^4]} \tag{33}$$

Typical oxygen and hydrogen line values for Eq. (29) are 102 $\frac{ft/sec}{BTU/lb_m}$ and 19 $\frac{ft/sec}{BTU/lb_m}$, respectively. A factor of five difference between the propellant lines' values results from the large enthalpy decrease in the fuel line as compared to the oxygen line. Typical values of Eq. (30) are simply the negative of those for Eq. (29). Eq. (31), the partial derivative of throat velocity with respect to line density, has typical values of -0.24 $\frac{ft/sec}{lb_m/ft^3}$ and -31 $\frac{ft/sec}{lb_m/ft^3}$ for the oxygen and hydrogen lines, respectively. The two orders of magnitude difference results from two causes. One is the throat velocity term in the numerator of Eq. (31). Oxidizer velocity at the venturi throat is 250 ft/sec compared to the fuel line's 1340 ft/sec, a factor of five difference. The other cause is that the density expression in Eq. (31) has a value of 0.24 for the oxygen line and 6.85 for the hydrogen line, approximately a factor of 20 difference. Typical values for Eq. (32), the partial derivative of throat velocity with respect to throat density, are different by two orders of magnitude also (0.25 $\frac{ft/sec}{lb_m/ft^3}$ for the oxygen line and 32 $\frac{ft/sec}{lb_m/ft^3}$ for hydrogen line) for the same reasons mentioned above. Lastly, the throat velocity partial derivative with respect to the line contraction coefficient, Eq. (33), has typical values of 7.5 and 49.5 for the oxidizer and fuel lines, respectively with units of ft/sec. The factor of five difference is primarily a result of the comparison of the values of throat velocity between the two propellant lines.

To attain the partial derivatives of venturi throat velocity with respect to the measured quantities, the following equations are applied:

$$\frac{\partial V_{th}}{\partial p_{line}} = \frac{\partial V_{th}}{\partial h_{line}}\frac{\partial h_{line}}{\partial p_{line}} + \frac{\partial V_{th}}{\partial h_{th}}\frac{\partial h_{th}}{\partial p_{line}} + \frac{\partial V_{th}}{\partial \rho_{line}}\frac{\partial \rho_{line}}{\partial p_{line}} + \frac{\partial V_{th}}{\partial \rho_{th}}\frac{\partial \rho_{th}}{\partial p_{line}} \tag{34}$$

$$\frac{\partial V_{th}}{\partial dp} = \frac{\partial V_{th}}{\partial h_{th}}\frac{\partial h_{th}}{\partial dp} + \frac{\partial V_{th}}{\partial \rho_{th}}\frac{\partial \rho_{th}}{\partial dp} \tag{35}$$

$$\frac{\partial V_{th}}{\partial T_{line}} = \frac{\partial V_{th}}{\partial h_{line}}\frac{\partial h_{line}}{\partial T_{line}} + \frac{\partial V_{th}}{\partial h_{th}}\frac{\partial h_{th}}{\partial T_{line}} + \frac{\partial V_{th}}{\partial \rho_{line}}\frac{\partial \rho_{line}}{\partial T_{line}} + \frac{\partial V_{th}}{\partial \rho_{th}}\frac{\partial \rho_{th}}{\partial T_{line}} \tag{36}$$

$$\frac{\partial V_{th}}{\partial d_{line}} = \frac{\partial V_{th}}{\partial \beta}\frac{\partial \beta}{\partial d_{line}} \tag{37}$$

$$\frac{\partial V_{th}}{\partial d_{th}} = \frac{\partial V_{th}}{\partial \beta}\frac{\partial \beta}{\partial d_{th}} \tag{38}$$

Values for the oxygen and hydrogen line partial with respect to line pressure were -0.19 $\frac{ft/sec}{psia}$ and -1.05 $\frac{ft/sec}{psia}$. Equation (35) results in values of 4.9 and 16.5 for the oxidizer and fuel lines, respectively with units of $\frac{ft/sec}{psia}$. The partial derivative with respect to line temperature yielded values of 0.28 $\frac{ft/sec}{R}$ and 1.25 $\frac{ft/sec}{R}$ for the oxygen and hydrogen lines. Equation (37), the line

diameter partial gave oxygen and hydrogen values of -1.2 and -8.3, and Eq. (38), the venturi throat diameter partial, resulted in values of 4.6 and 30.7 for the oxidizer and fuel propellant lines, respectively, all having units of $\frac{ft/sec}{inches}$.

Propellant mass flow rate. There are three partial derivatives of the mass flow rate of each propellant.

$$\frac{\partial \dot{m}}{\partial d_{th}} = C_d \frac{\pi}{4} \rho_{th} (d_{th}^2 \frac{\partial V_{th}}{\partial d_{th}} + 2 d_{th} V_{th}) \tag{39}$$

$$\frac{\partial \dot{m}}{\partial \rho_{th}} = C_d \frac{\pi}{4} d_{th}^2 (\rho_{th} \frac{\partial V_{th}}{\partial d_{th}} + V_{th}) \tag{40}$$

$$\frac{\partial \dot{m}}{\partial V_{th}} = C_d \frac{\pi}{4} d_{th}^2 \rho_{th} \tag{41}$$

Eq. (39), the partial derivative of propellant mass flow rate with respect to the venturi throat diameter, has typical values of 4.0 $\frac{lb_m/sec}{inches}$ and 1.3 $\frac{lb_m/sec}{inches}$ for the oxygen and hydrogen lines, respectively. A factor of five difference exists between the oxygen and hydrogen line values of Eq. (40), the partial derivative with respect to throat density (the values are .21 and 1.4, respectively with units of $\frac{lb_m/sec}{lb_m/ft^3}$), due to the throat velocity term in the numerator of the expression. The last propellant mass flow rate partials is the throat velocity influence on propellant mass flow rate. Typical values are 0.003 for the oxygen line and 0.0002 for the hydrogen line with units of $\frac{lb_m/sec}{ft/sec}$. The very large value of the oxygen line density is the cause of the difference between values.

As in the case of venturi throat velocity, the influence coefficients of the propellant mass flow rate need to be expressed with respect to the quantities which were actually measured. The following expressions were used to calculate the required coefficients:

$$\frac{\partial \dot{m}}{\partial p_{line}} = \frac{\partial \dot{m}}{\partial V_{th}} \frac{\partial V_{th}}{\partial p_{line}} + \frac{\partial \dot{m}}{\partial \rho_{th}} \frac{\partial \rho_{th}}{\partial p_{line}} \tag{42}$$

$$\frac{\partial \dot{m}}{\partial T_{line}} = \frac{\partial \dot{m}}{\partial V_{th}} \frac{\partial V_{th}}{\partial T_{line}} + \frac{\partial \dot{m}}{\partial \rho_{th}} \frac{\partial \rho_{th}}{\partial T_{line}} \tag{43}$$

$$\frac{\partial \dot{m}}{\partial dp} = \frac{\partial \dot{m}}{\partial V_{th}} \frac{\partial V_{th}}{\partial dp} + \frac{\partial \dot{m}}{\partial \rho_{th}} \frac{\partial \rho_{th}}{\partial dp} \tag{44}$$

$$\frac{\partial \dot{m}}{\partial d_{line}} = \frac{\partial \dot{m}}{\partial V_{th}} \frac{\partial V_{th}}{\partial d_{line}} \tag{45}$$

Values for the line pressure partial, Eq. (42), were 0.0007 and 0.0002 $\frac{ft/sec}{psia}$ for the oxidizer and fuel lines, respectively. Equation (43), the partial with respect to line temperature, had values of -0.0009 and -0.0002 $\frac{ft/sec}{R}$ for the oxygen and hydrogen propellants, respectively. The partial derivatives with respect to differential pressure took values of 0.015 and 0.0032 $\frac{ft/sec}{psia}$ for the oxygen and fuel side, respectively. Each propellant's mass flow rate partial derivative with respect to propellant line diameter have values of -0.0039 and -0.0018 $\frac{ft/sec}{inches}$.

Total mass flow rate. Like the throat pressure equation, the partials for the total mass flow rate were simply calculated as:

$$\frac{\partial \dot{m}_{TOT}}{\partial \dot{m}_{ox}} = 1 \tag{46}$$

$$\frac{\partial \dot{m}_{TOT}}{\partial \dot{m}_{fu}} = 1 \tag{47}$$

This results from the purely additive nature of the calculation, Eq. (19). Calculating the influence coefficients which relate back to the propellant line temperatures, line pressures, and differential pressures result in:

$$\frac{\partial \dot{m}_{TOT}}{\partial p_{line}} = \frac{\partial \dot{m}_{TOT}}{\partial \dot{m}} \frac{\partial \dot{m}}{\partial p_{line}} \tag{48}$$

$$\frac{\partial \dot{m}_{TOT}}{\partial T_{line}} = \frac{\partial \dot{m}_{TOT}}{\partial \dot{m}} \frac{\partial \dot{m}}{\partial T_{line}} \tag{49}$$

$$\frac{\partial \dot{m}_{TOT}}{\partial dp} = \frac{\partial \dot{m}_{TOT}}{\partial \dot{m}} \frac{\partial \dot{m}}{\partial dp} \tag{50}$$

$$\frac{\partial \dot{m}_{TOT}}{\partial d_{line}} = \frac{\partial \dot{m}_{TOT}}{\partial \dot{m}} \frac{\partial \dot{m}}{\partial d_{line}} \tag{51}$$

$$\frac{\partial \dot{m}_{TOT}}{\partial d_{th}} = \frac{\partial \dot{m}_{TOT}}{\partial \dot{m}} \frac{\partial \dot{m}}{\partial d_{th}} \tag{52}$$

Each of these equations must be applied to the oxygen and fuel lines. Since the values of Eqs. (46) and (47) are unity, the values for the expressions are the same as those given for Eq. (39) and Eqs. (42) through (45).

Vacuum thrust. Influence coefficients for the vacuum thrust equation were simple to calculate, and are expressed below.

$$\frac{\partial F_{vac}}{\partial F_{site}} = 1 \tag{53}$$

$$\frac{\partial F_{vac}}{\partial p_{amb}} = A_{exit} \tag{54}$$

$$\frac{\partial F_{vac}}{\partial A_{exit}} = p_{amb} \tag{55}$$

Eq. (53) reflects the fact that a unit change in site thrust is directly converted to a unit change in vacuum thrust. However, Eqs. (54) shows that a 1 *psia* change in ambient pressure causes a 816 lb_f change in vacuum thrust. Likewise, a 1 $inch^2$ change in nozzle exit area causes a 0.036 lb_f change in vacuum thrust. Since the quantities used to compute the vacuum thrust were all measured quantities, there was no reason to calculate more partials derivatives using the chain rule as was the case of the venturi throat velocity and the mass flow quantities.

Vacuum specific impulse. Two influence coefficients result from the specific impulse calculation.

$$\frac{\partial I_{sp}}{\partial F_{vac}} = \frac{1}{\dot{m}_{TOT}} \tag{56}$$

$$\frac{\partial I_{sp}}{\partial \dot{m}_{TOT}} = -\frac{F_{vac}}{\dot{m}_{TOT}^2} \tag{57}$$

Typical values are 0.90 $\frac{sec}{lb_f}$ and -0.43 $\frac{sec}{lb_m/sec}$ for Eqs. (56) and (57), respectively. To express the partials with respect to measured quantities, the following equations were used:

$$\frac{\partial I_{sp}}{\partial p_{line}} = \frac{\partial I_{sp}}{\partial \dot{m}_{TOT}} \frac{\partial \dot{m}_{TOT}}{\partial p_{line}} \tag{58}$$

$$\frac{\partial I_{sp}}{\partial T_{line}} = \frac{\partial I_{sp}}{\partial \dot{m}_{TOT}} \frac{\partial \dot{m}_{TOT}}{\partial T_{line}} \tag{59}$$

$$\frac{\partial I_{sp}}{\partial dp} = \frac{\partial I_{sp}}{\partial \dot{m}_{TOT}} \frac{\partial \dot{m}_{TOT}}{\partial dp} \tag{60}$$

$$\frac{\partial I_{sp}}{\partial d_{line}} = \frac{\partial I_{sp}}{\partial \dot{m}_{TOT}} \frac{\partial \dot{m}_{TOT}}{\partial d_{line}} \tag{61}$$

$$\frac{\partial I_{sp}}{\partial d_{th}} = \frac{\partial I_{sp}}{\partial \dot{m}_{TOT}} \frac{\partial \dot{m}_{TOT}}{\partial d_{th}} \tag{62}$$

$$\frac{\partial I_{sp}}{\partial F_{site}} = \frac{\partial I_{sp}}{\partial F_{vac}} \frac{\partial F_{vac}}{\partial F_{site}} \tag{63}$$

$$\frac{\partial I_{sp}}{\partial p_{amb}} = \frac{\partial I_{sp}}{\partial F_{vac}} \frac{\partial F_{vac}}{\partial p_{amb}} \tag{64}$$

$$\frac{\partial I_{sp}}{\partial A_{exit}} = \frac{\partial I_{sp}}{\partial F_{vac}} \frac{\partial F_{vac}}{\partial A_{exit}} \tag{65}$$

Values for the line pressure partial derivative were −0.3 and −0.1 $\frac{sec}{psia}$ for the oxygen and fuel sides, respectively. Oxygen and hydrogen line temperature partials took on values of 0.40 and 0.12 $\frac{sec}{R}$. Specific impulse partial derivatives with respect to differential pressure had values of −6.66 and −1.39 for the oxidizer and fuel sides, respectively with units of $\frac{sec}{psia}$. The partial with respect to line diameter had values of 1.67 and 0.78 $\frac{sec}{inches}$ and for the venturi throat diameter, −1732.0 and −577.9 $\frac{sec}{inches}$, for the oxygen and hydrogen lines, respectively. A unit change in the site thrust value had a 0.9 $\frac{sec}{lb_f}$ effect on specific impulse. The partial with respect to ambient pressure was 732.9 $\frac{sec}{psia}$ and with respect to nozzle exit area was 0.0325 $\frac{sec}{inches^2}$.

A sample calculation of the determination of the influence coefficient, error propagation, and final uncertainty computation for a simple case, the oxygen line contraction ratio, β_{ox}, is given in Appendix B.

Data Used in Study

The data which were selected results for this type of experimental set-up was collected at the NASA RETF during the winter of 1986. Gaseous hydrogen and gaseous oxygen were the rocket engine's respective fuel and oxidizer. Attached to the rocket engine combustion chamber was an optimized Rao contour nozzle which had been designed with an inviscid core area ratio of 1000:1 and had been boundary layer corrected to an area ratio of 1030:1.

Elemental Error Sources

Before propagating errors from different instruments through the data reduction equations using the appropriate influence coefficients, an exhaustive list of possible error sources was compiled. The list is categorized by measurement device (pressure transducer, temperature thermocouple, and force transducer) and is subdivided into calibration and data acquisition errors.

Pressure measurements (Table IV). The elemental sources of error for pressure and differential pressure transducers are combined. Zero reading errors in all pressure transducers were eliminated by numerically zeroing the instruments before taking data. Traceability of the transducer calibration from the standards lab to the National Bureau of Standards (NBS) was accounted for with NBS calibration reports on lab standard instruments. Errors due to changes in transducer calibration

pressure were eliminated by calibrating the instruments at test conditions. Transducer hysteresis and nonlinearity were determined by independent calibration of the instruments.

Possible sources of data acquisition errors in pressure measurements, aside from data scatter, were manifested in the following ways. Transducer temperature differences at the time of zero balancing and data-taking are considered negligible because the propellant lines were at room temperature at all times. Errors due to the determination of a reference pressure were determined by an independent calibration. Changes in line temperature and pressure were determined to have a negligible effect on the transducer because they were at room temperature and experienced very small pressure changes during the tests. Damping of the propellant lines eliminated the effect of vibration on the transducer.

Temperature measurements (Table V). Calibration errors for temperature thermocouples were characterized by the following errors. Specifications by the manufacturer identified wire calibration and reference temperature level determination errors.

Data acquisition errors of the temperature measurement system included the following elements. Errors due to thermocouple temperature difference were assumed to be negligible because the propellant lines were at room temperature at all times. Fabrication of the thermocouples were according to accepted standard practices and it was assumed that no errors were introduced as a result. Effects of vibration on the thermocouple were assumed to be negligible because the propellant lines were damped. Because line pressure changes were negligible during testing, errors due to this source were neglected. Reference temperature stability was specified by the manufacturer to be $\pm$ 0.25%. Errors in thermocouple design due to radiation, friction, etc., when measuring gas temperatures were assumed to be minimized due to good thermocouple design practices. Heat conduction error sources and errors due to temperature gradients along non-homogeneous thermocouple wire were assumed to be negligible.

Force measurements (Table VI). Calibration error in force measurements, including the following sources, were assessed. Errors due to the standards lab calibration of the transducer, including NBS traceability, were determined to be the error of the standards lab's calibration instruments. Thrust stand hysteresis and non-linearity were determined experimentally to be $\pm$ 0.5% full scale. Errors due to a shift in load cell calibration caused by the attachment of adaptors and flexures were compensated for by in situ calibrations.

Data acquisition errors which were addressed are listed below. Zero reading error was eliminated because the instruments were numerically zeroed before data taking. Vibration effects on the load cell and on the thrust stand were detemined to be negligible due to the design of the facility. Errors resulting from the misalignment between the engine force vector and the force vector measured by the data load cell train were minimized by using a triad of transducers in a parallel configuration. Similarly, the triad arrangement of force transducers accounts for misalignment of forces on an axis different from the engine centerline. Errors introduced due to pressurization on the load cell were corrected by aneroid calibration (ref. 28). Cell pressure effects on the cell wall were neglected because the cell wall was not the ground for the load cell. Errors due to the effect of changes in line pressure on the tare forces exerted on the thrust measurement system by propellant lines routed to the engine are reduced to a negligible magnitude by the physical set-up of the experiment. Effect of changes in temperature on the load cell was negligible because temperature changes were very small during calibration and testing. Similarly, thermal growth of the thrust stand errors were negligible also. Errors due to secondary airflow effects on the load cell were negligible during steady state operation of the engine.

Error sources common to all instruments. In common to all the measurement devices were the following error source considerations. Error in the ability to determine a representative data value over a specified time interval as the data varied was reduced by averaging over five samples taken at 50 Hertz intervals and characterizing these averages by a line of best fit. Errors introduced through

signal conditioning, electrical calibration, and digital systems were approximated with data from other test facilities at NASA LeRC.

RESULTS

By applying the methodology described and through the use of the equations listed, an uncertainty analysis was performed for the rocket engine test program conducted at the NASA Lewis RETF. A listing of the parameters measured and calculated, their nominal value, the amount of precision error in each, their associated degrees of freedom, the value of uncertainty, and their uncertainty expressed as a percentage, are tabulated in table VII. Most worthy of notice is the uncertainty value of specific impulse as a percentage. The test facility configured as described in this report is capable of measuring the specific impulse within 1.30%. Other parameters, such as vacuum thrust and total mass flow rate, were measured to within 1.12% and 0.72%, respectively.

In order to appreciate which error sources most contribute to the specific impulse error, each term of the overall specific impulse precision error equation is expanded in table VIII. Each measured parameter's calibration and data acquisition error value is listed (in columns 2 and 4) as well as the influence coefficient of specific impulse taken with respect to that measured parameter (column 1). The product of the influence coefficient and the associated error component (calibration or data acquisition) results in the amount of error, in units of specific impulse, which can be attributed to each measured parameter (columns 3 and 5). In presenting the data in this manner, the largest contributors to overall specific impulse error are easily seen. Table VIII shows readily that the calibration error is the major portion of the overall specific impulse error, indicating that the calibration process should be improved to effect the largest gains in specific impulse measurement accuracy. Within the category of calibration errors, the largest component of error is due to the ambient pressure transducer with over 43% of the total specific impulse calibration error. Another 26% is contributed by the measured site thrust measurement. The next measurement which most affects the specific impulse calibration error is the oxygen venturi throat diameter with 14%. Therefore, the calibration errors of these three measurement devices are the cause of approximately 83% of the total specific calibration error. The six largest contributors to calibration error combine to comprise approximately 90% of the total error. Hence, to improve the overall uncertainty of specific impulse, better calibration of the these three instruments would effect the largest improvement.

CONCLUSIONS

An uncertainty analysis was conducted for the High Area Ratio Nozzle test program tests which were run during the winter of 1986 at the NASA Lewis Rocket Engine Test Facility (RETF). The standardized uncertainty methodology, as described by Abernethy (ref. 1), was followed. The data reduction equations were described and the expressions which define the influence coefficients were explained in detail. Elemental error sources of all types of measurements were discussed.

A comparison of influence coefficients as determined by this analysis with similar coefficients, calculated with the data reduction program used in the experiment, was used to verify the uncertainty analysis model. In this way, the use of influence coefficients which were not taken with respect to the originally measured parameters were determined to be in error for use with this analysis. Their use leads to largely inflated results and caution should be taken to verify the influence coefficients values with independent computer programs whenever possible.

Total uncertainty on specific impulse was determined to be 1.30%. Uncertainty on total mass flow rate was 0.72% and on vacuum thrust was 1.12%.

To continue the study of uncertainty analysis as it applies to rocket engine tests, the inclusion of estimates for the small bias errors of unknown magnitude for all instrumentation would provide better estimates of uncertainty in the performance parameters of interest to the rocket engine community.

APPENDIX A

List of Symbols

A	Area, $inches^2$	s	Entropy, $BTU/lb_m/R$
B	Bias error	SEE	Standard estimate of error
C	Number of constants in a curve-fit	T	Temperature, R
C_d	Venturi discharge coefficient	t_{95}	Student's t value
d	Diameter, *inches*	U_{95}	Uncertainty range encompassing 95% of data
dp	Static pressure difference between the propellant line and the venturi throat	U_{99}	Uncertainty range encompassing 99% of data
F	Thrust, lb_f	V	Velocity, ft/sec
h	Enthalpy, BTU/lb_m	X	Variable
I_{sp}	Specific impulse, sec	$\overline{X}$	Average over all X values
K	Conversion factor, 50079.5 $[(ft/sec)^2/(BTU/lb_m)]$	y	Parameter
$\dot{m}$	Mass flow rate, lb_m/sec	β	Propellant line contraction ratio
N	Number of points in test	θ	Influence Coefficients
P	Parameters	ν	Degrees of freedom
p	Static pressure, *psia*	π	3.14159
r	Computed result	ρ	Density, lb_m/ft^3
S	Precision error	ϕ	Generalized thermodynamic property variable

Subscripts

c	Calculated	*site*	Site
cal	Calibration	*th*	Venturi throat station
da	Data Acquisition	*TOT*	Total (i.e., combined propellants)
exit	Nozzle exit plane station	*vac*	Vacuum
i	index	p	Pooled
line	Propellant line station	X	Variable

APPENDIX B

Sample Calculation

To demonstrate the calculation procedure, a simple example was chosen for which the given data is presented, the influence coefficients are calculated, the errors are propagated, and the uncertainty is determined. The oxygen line contraction ratio was chosen to illustrate the computation procedures discussed in this report.

Given Data:

$d_{line,ox} = 1.61\ inches$

$d_{th,ox} = 0.406\ inches$

$\nu_{d_{line,ox}} = 30$

$\nu_{d_{th,ox}} = 30$

$S_{cal,d_{line,ox}} = 0.0001\ inches$

$S_{cal,d_{th,ox}} = 0.00065\ inches$

$S_{da,d_{line,ox}} = 0\ inches$

$S_{da,d_{th,ox}} = 0\ inches$

Calculation of Contraction Ratio, β

$$\beta_{ox} = \frac{d_{th,ox}}{d_{line,ox}}$$

$$\beta_{ox} = \frac{(0.406)}{(1.61)} = 0.252$$

Calculation of Influence Coefficients

$$\frac{\partial \beta_{ox}}{\partial d_{line,ox}} = -\frac{d_{th,ox}}{d_{line,ox}^2}$$

$$\frac{\partial \beta_{ox}}{\partial d_{line,ox}} = -\frac{(0.406)}{(1.61)^2} = -0.157\ inches^{-1}$$

$$\frac{\partial \beta_{ox}}{\partial d_{th,ox}} = \frac{1}{d_{line,ox}}$$

$$\frac{\partial \beta_{ox}}{\partial d_{line,ox}} = \frac{1}{1.61} = 0.621\ inches^{-1}$$

Propagation of Precision Errors

Calibration Errors:

$$S_{cal,\beta_{ox}} = \sqrt{(\frac{\partial \beta_{ox}}{\partial d_{line,ox}} S_{cal,d_{line,ox}})^2 + (\frac{\partial \beta_{ox}}{\partial d_{th,ox}} S_{cal,d_{th,ox}})^2}$$

$$S_{cal,\beta_{ox}} = \sqrt{(-0.157 \times 0.0001)^2 + (0.621 \times 0.00065)^2}$$

$$S_{cal,\beta_{ox}} = \sqrt{(2.47 \times 10^{-10}) + (1.63 \times 10^{-7})}$$

$$S_{cal,\beta_{ox}} = 4.04 \times 10^{-4}$$

Data Acquisition Errors:

$$S_{da,\beta_{ox}} = \sqrt{(\frac{\partial \beta_{ox}}{\partial d_{line,ox}} S_{da,d_{line,ox}})^2 + (\frac{\partial \beta_{ox}}{\partial d_{th,ox}} S_{da,d_{th,ox}})^2}$$

$$S_{da,\beta_{ox}} = \sqrt{(-0.157 \times 0 + (0.621 \times 0)}$$

$$S_{da,\beta_{ox}} = 0$$

Combination of Errors:

$$S_{\beta_{ox}} = \sqrt{S^2_{cal,\beta_{ox}} + S^2_{da,\beta_{ox}}}$$

$$S_{\beta_{ox}} = \sqrt{(4.04 \times 10^{-4})^2 + 0^2}$$

$$S_{\beta_{ox}} = 4.04 \times 10^{-4}$$

Calculation of the Degrees of Freedom

$$\nu_{\beta_{ox}} = \frac{\left(\sum_{i=1}^{N} S_i^2\right)^2}{\sum_{i=1}^{N} \frac{S_i^4}{\nu_i}}$$

$$\nu_{\beta_{ox}} = \frac{[(\frac{\partial \beta_{ox}}{\partial d_{line,ox}} S_{d_{line,ox}})^2 + (\frac{\partial \beta_{ox}}{\partial d_{th,ox}} S_{d_{th,ox}})^2]^2}{\left[(\frac{\partial \beta_{ox}}{\partial d_{line,ox}} S_{d_{line,ox}})^4 / \nu_{d_{line,ox}} + (\frac{\partial \beta_{ox}}{\partial d_{th,ox}} S_{d_{th,ox}})^4 / \nu_{d_{th,ox}}\right]}$$

$$\nu_{\beta_{ox}} = \frac{[(-0.157 \times 0.0001)^2 + (0.621 \times 0.00065)^2]}{[(-0.157 \times 0.0001)^4/30 + (0.621 \times 0.00065)^4/30]}$$

$$\nu_{\beta_{ox}} = \frac{[2.47 \times 10^{-10} + 1.63 \times 10^{-7}]^2}{[2.03 \times 10^{-21} + 8.87 \times 10^{-16}]}$$

$$\nu_{\beta_{ox}} = \frac{2.665 \times 10^{-14}}{8.87 \times 10^{-16}} = 30.06 \doteq 30$$

Calculation of Uncertainty

From Table I, the Student's t value corresponding to $\nu_{\beta_{ox}} = 30$ is $t_{95} = 2$.

$$U_{99,\beta_{ox}} = \pm t_{95} S_{\beta_{ox}} = \pm 2 \times (4.04 \times 10^{-4})$$

$$U_{99,\beta_{ox}} = 8.08 \times 10^{-4}$$

To express the uncertainty as a percentage of the nominal value:

$$U_{99,\beta_{ox}}\% = \frac{U_{99,\beta_{ox}}}{\beta_{ox}} \times 100$$

$$U_{99,\beta_{ox}}\% = \frac{8.08 \times 10^{-4}}{0.252} \times 100 = 0.321\%$$

REFERENCES

1. Abernethy, R.B.; et. al: ICRPG Handbook for Estimating the Uncertainty in Measurements Made With Liquid Propellant Rocket Engine Systems. JANNAF (formerly ICRPG) Performance Standardization Working Group Report CPIA No. 180 (AD 851 127), April 1969.

2. Praharaj, S.C. and Palko, R.L.; "Measurements for Rocket Engine Performance Code Verification." Report RTR 157-01, REMTECH, Inc., Oct. 1986.

3. Ku, H.H.: Uncertainty is NBS's Business. Presented to the NBA Advisory Panel, October 9, 1975.

4. Abernethy, R.B., et al: Handbook Uncertainty in Gas Turbine Measurements. USAF Arnold Engineering Development Center, Report AEDC-TR-73-5, February 1973. (AD-755 356)

5. Ku, H.H.: Precision Measurement and Calibration. NBS Special Publication 300, Volume 1, 1969.

6. Rosenblatt, J.; and Spiegelman, C.H.: Discussion. NBS, Technometric Volume 23, No. 4, November 1981.

7. Letter Dr. Joan R. Rosenblatt, Director Center for Applied Mathematics, NBS to Dr. Robert B. Abernaethy, December 8, 1980 and NBS Special Publication 644, Expression of the Uncertainties of Final Measurement Results: Reprints, January 1983.

8. Hersey, M.D.: A Development of the Theory of Errors with Reference to Economy of Time. British Association for the Advancement of Science, 1913, Reprinted by Churchill Eisenhart, NBS, Journal of Researtch, 1965.

9. Kline, S.J. and McClintock, F.A.: Describing Uncertainties in Single-Sample Experiments. Mechanical Engineering, Volume 75, 1953.

10. MIDAP Study Group: Guide to In-Flight Thrust Measurement of Turbojets and Turbofans. Agardograph AG-237, January, 1979.

11. Measurement of a Fluid Flow-Estimation of Uncertainty of a Flow-Rate Measurement, ISO 5168, 1976.

12. Abernethy, R.B.: SAE In-Flight Propulsion Measurement Committee E33: Its Life and Work. SAE in Aerospace Engineering Volume 1, No. 1., July 1981.

13. Abernethy, R.B., et al: Measurement Uncertainty Handbook, ISBM: 87664-483-3, Revised 1980. Instrument Society of America.

14. Golden, R.W.: Semiscale Uncertainty Report: Methodology. Prepared for U.S. Nuclear Regulatory Commission, MUREG/CR-2459, September 1982.

15. Schumacher, P.B.F.: Systematic Measurement Errors, ASQC Journal of Quality Technology, January 1981.

16. American National Standard for Calibration Systems, ASQC Writing Group Draft, 1983.

17. Measurement Uncertainty, ANSI/ASME PTC 19.1, 1984, Performance Test Codes Supplement.

18. Measurement Uncertainty for Fluid Flow in Closed Conduits, ANSI/ASME MFC-2M, 1983.

19. Abernethy, R.B.; Benedict, R.P.; and Dowdell, R.B.: ASME Measurement Uncertainty. ASME paper 83-WA/FM-3.

20. Conducting an Interlaboratory Test Program to Determine the Precision of Test Methods, ASTM/ANSI E691-79.

21. Berkson, J: Are There Two Regressions?. American Statistical Association Journal, June 1950.

22. VIM: International Vocabulary of Basic and General Terms in Metrology, BIPM-ISO-CEI-OIML, VIM Working Group 1983.

23. Campion, P.J.; Burns, J.E.; Williams, A.: A Code of Practice for the Detailed Statement of Accuracy. National Physics Laboratory, Great Britain, 1973.

24. Hayward, A.T.J.: Repeatability and Accuracy. Mechanical Engineering Publications Limited 1977.

25. Abernethy, R.B.; et al: Uncertainty Methodology for in-Flight Thrust Determination. SAE paper 831436, October 1983, see also SAE paper 831439 for application.

26. Smith, Jr., R.E.; Wehofer, S.: From Measurement Uncertainty to Measurement Communitcations, Credibility and Cost Control. . ..Sverdrup, Tullahoma, Tennessee 37389, ASME paper 1983 WAM.

27. ASME PTC 19.1, Performance Test Codes Measurement Uncertainty, 1986.

28. Pavli, A.J.; Kacynski, K.J.; and Smith, T.A.: Experimental Thrust Performance of a High-Area-Ratio Rocket Nozzle. NASA TP-2720, 1987.

29. Hendricks, R.C.; Baron, A.K.; and Peller, I.C.: GASP - A Computer Code for Calculating the Thermodynamic and Transport Properties for Ten Fluids: Parahydrogen, Helium, Neon, Methane, Nitrogen, Carbon Monoxide, Oxygen, Fluorine, Argon, and Carbon Dioxide. NASA TN D-7808, 1975.

30. Davidian, K.J.: Pretest Uncertainty Analysis for Chemical Rocket Engine Tests. NASA TM-89819, 1987.

TABLE I. DEGREES OF FREEDOM, ν, AND ASSOCIATED STUDENT'S T VALUE, t_{95}

ν	t_{95}	ν	t_{95}	ν	t_{95}	ν	t_{95}	ν	t_{95}	ν	t_{95}
1	12.706	6	2.447	11	2.201	16	2.120	21	2.080	26	2.056
2	4.303	7	2.365	12	2.179	17	2.110	22	2.074	27	2.052
3	3.182	8	2.306	13	2.160	18	2.101	23	2.069	28	2.048
4	2.776	9	2.262	14	2.145	19	2.093	24	2.064	29	2.045
5	2.571	10	2.228	15	2.131	20	2.086	25	2.060	≥ 30	2.000

TABLE II. INFLUENCE COEFFICIENTS OF THERMODYNAMIC PROPERTIES IN THE PROPELLANT LINE

Influence Coefficients	Oxygen Line	Hydrogen Line	Units
$\partial h_{line}/\partial p_{line}$	-0.790×10^{-2}	0.104×10^{-1}	$\frac{BTU/lb_m}{lb_f/in^2}$
$\partial h_{line}/\partial T_{line}$	$0.239 \times 10^{+0}$	$0.358 \times 10^{+1}$	$\frac{BTU/lb_m}{R}$
$\partial \rho_{line}/\partial p_{line}$	0.622×10^{-2}	0.335×10^{-3}	$\frac{lb_m/ft^3}{lb_f/in^2}$
$\partial \rho_{line}/\partial T_{line}$	-0.896×10^{-2}	-0.406×10^{-3}	$\frac{lb_m/ft^3}{R}$
$\partial s_{line}/\partial p_{line}$	-0.107×10^{-3}	-0.156×10^{-2}	$\frac{BTU/lb_m/R}{lb_f/in^2}$
$\partial s_{line}/\partial T_{line}$	0.467×10^{-3}	0.671×10^{-2}	$\frac{BTU/lb_m/R}{lb_f/in^2}$

TABLE III. INFLUENCE COEFFICIENTS OF THERMODYNAMIC PROPERTIES AT THE VENTURI THROAT

Influence Coefficients	Oxygen Line	Hydrogen Line	Units
$\partial h_{th}/\partial p_{th}$	0.485×10^{-1}	$0.886 \times 10^{+0}$	$\frac{BTU/lb_m}{lb_f/in^2}$
$\partial h_{th}/\partial s_{line}$	$0.505 \times 10^{+3}$	$0.524 \times 10^{+3}$	$\frac{BTU/lb_m}{BTU/lb_m/R}$
$\partial \rho_{th}/\partial p_{th}$	0.421×10^{-2}	0.246×10^{-3}	$\frac{lb_m/ft^3}{lb_f/in^2}$
$\partial \rho_{th}/\partial s_{line}$	$-0.187 \times 10^{+2}$	-0.575×10^{-1}	$\frac{lb_m/ft^3}{BTU/lb_m/R}$
$\partial T_{th}/\partial p_{th}$	$0.238 \times 10^{+0}$	$0.244 \times 10^{+0}$	$\frac{R}{lb_f/in^2}$
$\partial T_{th}/\partial s_{line}$	$0.212 \times 10^{+4}$	$0.146 \times 10^{+3}$	$\frac{R}{BTU/lb_m/R}$

TABLE IV. SOURCES OF ELEMENTAL ERROR IN PRESSURE MEASUREMENTS

Calibration errors due to...	Comments
Zero reading error	Instruments are zeroed before data-taking
Standards lab calibration of the transducer calibration, including NBS traceability	Errors of standards lab's instruments
Changes in transducer calibration pressure	Not applicable
Transducer hysteresis	Independent calibration
Transducer nonlinearity	Independent calibration
Data acquisition errors due to...	**Comments**
Transducer temperature difference at zero balance	Negligible because lines were at room temperature
Transducer temperature difference at data-taking	Negligible because lines were at room temperature
Determination of reference pressure	Independent calibration
Changes in temperature of the transducer	Negligible because lines were at room temperature
Effect of vibration on the transducer	Negligible because propellant lines were damped
Effect of changes in line pressure	Line pressure changes were negligible during testing
Ability to determine a representative value over a specified time interval as data varies	Data averaging reduces error to negligible magnitude
Signal conditioning, electrical calibrations, and digital system	Based on past data from other test facilities at NASA Lewis

TABLE V. SOURCES OF ELEMENTAL ERROR IN TEMPERATURE MEASUREMENTS

Calibration errors due to...	Comments
Manufacturer's specification of wire calibration	Manufacturer's specifications
Reference temperature level detemination	Manufacturer's specifications
Data acquisition errors due to...	**Comments**
T/C temperature difference	Negligible because lines were at room temperature
Fabrication of T/C	As per standards
Effect of vibration on the T/C	Negligible because propellant lines are damped
Effect of changes in line pressure	Line pressure changes were during testing negligible
Reference temperature stability	$\pm 0.25\%$
T/C design due to radiation, friction, etc., when measuring gas temperature	Good design practice reduces this to negligible magnitude
Heat conduction	All parts at uniform temperature
Temperature gradients along nonhomogeneous T/C wire	All parts at uniform temperature
Ability to determine a representative values over a specified time interval as data varies	Data averaging reduces error to negligible magnitude
Signal conditioning, electrical calibrations, and digital system	Based on past data from other test facilities at NASA Lewis

TABLE VI. SOURCES OF ELEMENTAL ERROR IN THRUST MEASUREMENTS

Calibration errors due to...	Comments
Standards lab calibration of the transducer calibration, including traceability to NBS	Errors of standards lab's instruments
Thrust stand hysteresis and non-linearity	±0.5% as per manufacturer's specifications
Shift in load cell calibration caused by attachement of adaptors/flexures	Compensated for with in situ calibrations
Data acquisition errors due to...	**Comments**
Zero reading error	Instruments are numerically zeroed before data-taking
Effect of vibration on the load cell	Negligible
Effect of vibration on the thrust stand	Negligible
Misalignment between the engine force vector and the force vector measured by the load cell train	Triad arrangement accounts for misalignment
Measurement of forces on an axis different from the engine centerline	Triad arrangement accounts for misalignment
Pressurization on the load cell	Corrected by aneroid calibration
Effect of changes in cell pressure on the test cell wall	Cell wall is not ground for load cell
Effect of changes in line pressure on tare exerted on thrust measurement system by propellant lines, etc., routed to the engine	Physical set-up reduces these to negligible magnitude
Effect of changes in temperature on the load cell	Temperature changes were negligible during calibration and testing
Thermal growth of the thrust stand	Negligible
Secondary airflow effect on the load cell	Negligible during steady-state operation
Ability to determine a representative value over a specified time interval as data varies	Data averaging reduces error to negligible magnitude
Signal conditioning, electrical calibrations, and digital system	Based on past data from other test facilities at NASA Lewis

TABLE VII. UNCERTAINTY OF MEASURED AND CALCULATED PARAMETERS (Part 1 of 2)

Parameter Name	[units]	Nominal Value $in[units]$ (1)	Precision Index (S) in [units] (2)	Deg. of Free ν (3)	Uncrtnty Value $t_{95} \times (2)$ in [units] (4)	Uncrtnty as % of Nom Val $\frac{(4)}{(1)} \times 100$ (5)
Oxygen Line Pressure	$(psia)$	649.40	1.567	5	4.028	0.620
Hydrogen Line Pressure	$(psia)$	639.30	7.275	5	18.704	2.926
Oxygen Line Temperature	(R)	510.80	0.078	5	0.202	0.039
Hydrogen Line Temperature	(R)	533.60	0.078	5	0.201	0.038
Oxygen Delta Pressure #1	$(psia)$	25.12	0.136	5	0.350	1.394
Hydrogen Delta Pressure #1	$(psia)$	41.57	0.302	5	0.775	1.865
Oxygen Delta Pressure #2	$(psia)$	25.26	0.137	5	0.351	1.389
Hydrogen Delta Pressure #2	$(psia)$	42.16	0.302	5	0.776	1.839
Oxygen Line Diameter	$(inches)$	1.61	0.000	30	0.000	0.000
Hydrogen Line Diameter	$(inches)$	1.61	0.000	30	0.000	0.000
Oxygen Venturi Throat Diameter	$(inches)$	0.41	0.001	30	0.001	0.320
Hydrogen Venturi Throat Diameter	$(inches)$	0.44	0.001	30	0.002	0.343
Site Thrust	(lb_f)	500.38	1.684	5	4.329	0.865
Nozzle Exit Area	$(inches^2)$	815.70	0.010	30	0.020	0.002
Ambient Pressure #1	$(psia)$	0.03	0.004	5	0.010	29.500
Ambient Pressure #2	$(psia)$	0.04	0.004	5	0.010	24.378
Average Ambient Pressure	$(psia)$	0.04	0.004	5	0.010	26.724
Oxygen Line Contraction Ratio	*none*	0.25	4×10^{-4}	30	0.001	0.320
Hydrogen Line Contraction Ratio	*none*	0.27	5×10^{-4}	30	0.001	0.343
Oxygen Line Density	(lb_m/ft^3)	3.92	0.010	5	0.026	0.653
Hydrogen Line Density	(lb_m/ft^3)	0.22	0.002	5	0.006	2.863
Oxygen Line Entropy	$(BTU/lb_m/R)$	1.28	2×10^{-4}	5	0.001	0.036
Hydrogen Line Entropy	$(BTU/lb_m/R)$	11.72	0.011	5	0.029	0.251
Oxygen Line Enthalpy	(BTU/lb_m)	224.09	0.026	8	0.061	0.027
Hydrogen Line Enthalpy	(BTU/lb_m)	1790.35	0.349	5	0.898	0.050

TABLE VII. UNCERTAINTY OF MEASURED AND CALCULATED PARAMETERS (Part 2 of 2)

Parameter Name	[units]	Nominal Value $in[units]$ (1)	Precision Index (S) in [units] (2)	Deg. of Free ν (3)	Uncrtnty Value $t_{95} \times$ (2) in [units] (4)	Uncrtnty as % of Nom Val $\frac{(4)}{(1)} \times 100$ (5)
Oxygen Throat Pressure #1	$(psia)$	624.28	1.602	5	4.119	0.660
Hydrogen Throat Pressure #1	$(psia)$	597.73	7.300	5	18.769	3.140
Oxygen Throat Density #1	(lb_m/ft^3)	3.82	0.010	5	0.026	0.673
Hydrogen Throat Density #1	(lb_m/ft^3)	0.21	0.002	5	0.006	3.012
Oxygen Throat Temperature #1	(R)	504.90	0.104	7	0.245	0.049
Hydrogen Throat Temperature #1	(R)	523.71	0.163	12	0.356	0.068
Oxygen Throat Enthalpy #1	(BTU/lb_m)	222.88	0.026	8	0.060	0.027
Hydrogen Throat Enthalpy #1	(BTU/lb_m)	1754.42	0.642	11	1.413	0.081
Oxygen Throat Pressure #2	$(psia)$	624.14	1.602	5	4.120	0.660
Hydrogen Throat Pressure #2	$(psia)$	597.14	7.300	5	18.769	3.143
Oxygen Throat Density #2	(lb_m/ft^3)	3.82	0.010	5	0.026	0.673
Hydrogen Throat Density #2	(lb_m/ft^3)	0.21	0.002	5	0.006	3.014
Oxygen Throat Temperature #2	(R)	504.87	0.104	7	0.246	0.049
Hydrogen Throat Temperature #2	(R)	523.57	0.164	12	0.358	0.068
Oxygen Throat Enthalpy #2	(BTU/lb_m)	222.88	0.026	8	0.060	0.027
Hydrogen Throat Enthalpy #2	(BTU/lb_m)	1753.90	0.646	11	1.421	0.081
Oxygen Throat Velocity #1	(ft/sec)	245.73	0.850	7	2.009	0.818
Hydrogen Throat Velocity #1	(ft/sec)	1344.67	9.043	8	20.854	1.551
Oxygen Throat Velocity #2	(ft/sec)	246.43	0.856	6	2.094	0.850
Hydrogen Throat Velocity #2	(ft/sec)	1354.40	9.055	8	20.880	1.542
Oxygen Mass Flow Rate #1	(lb_m/sec)	0.82	0.004	26	0.008	0.949
Hydrogen Mass Flow Rate #1	(lb_m/sec)	0.29	0.002	11	0.005	1.728
Oxygen Mass Flow Rate #2	(lb_m/sec)	0.82	0.003	26	0.008	0.953
Hydrogen Mass Flow Rate #2	(lb_m/sec)	0.30	0.002	11	0.005	1.728
Oxygen Average Mass Flow Rate	(lb_m/sec)	0.82	0.003	45	0.007	0.819
Hydrogen Average Mass Flow Rate	(lb_m/sec)	0.30	0.002	10	0.005	1.667
Total Mass Flow Rate	(lb_m/sec)	1.11	0.004	49	0.008	0.721
Vacuum Thrust	(lb_f)	529.89	2.771	14	5.943	1.122
Vacuum Specific Impulse	(sec)	476.10	3.023	29	6.183	1.299

TABLE VIII. SPECIFIC IMPULSE PRECISION ERROR BREAKDOWN

Parameter Name	[units]	Influence Coefficient *sec/[units]* (1)	Calib-ration Error [units] (2)	Calib-ration Value [sec] |(1) × (2)| (3)	Data Acqu. Error [units] (4)	Data Acqu. Value [sec] |(1) × (4)| (5)
Ambient Pressure #1	(*psia*)	366.40	0.004	1.376	2×10^{-4}	0.064
Ambient Pressure #2	(*psia*)	366.40	0.004	1.376	2×10^{-4}	0.064
Site Thrust	(lb_f)	0.8985	1.677	1.498	0.399	0.358
Oxygen Throat Diameter	(*inches*)	-1733.0	7×10^{-4}	1.126	0.000	0.000
Fuel Line Pressure	(*psia*)	-0.1069	7.272	0.777	0.566	0.061
Oxygen Line Pressure	(*psia*)	-0.0294	1.562	0.459	0.318	0.094
Oxygen Delta Pressure #1	(*psia*)	-3.341	0.132	0.441	0.088	0.295
Oxygen Delta Pressure #2	(*psia*)	-3.329	0.132	0.439	0.092	0.306
Fuel Throat Diameter	(*inches*)	-577.90	8×10^{-4}	0.433	0.000	0.000
Fuel Delta Pressure #1	(*psia*)	-0.697	0.301	0.210	0.049	0.034
Fuel Delta Pressure #2	(*psia*)	-0.691	0.301	0.208	0.051	0.035
Oxygen Line Temperature	(*R*)	0.3995	0.075	0.030	0.061	0.024
Fuel Line Temperature	(*R*)	0.1160	0.075	0.009	0.059	0.007
Nozzle Exit Area	($inches^2$)	0.0325	0.010	3×10^{-4}	6×10^{-5}	2×10^{-5}
Oxygen Line Diameter	(*inches*)	1.6730	0.000	0.000	0.000	0.000
Fuel Line Diameter	(*inches*)	0.7787	0.000	0.000	0.000	0.000
Root Sum Squared (RSS)				±2.963		±0.578

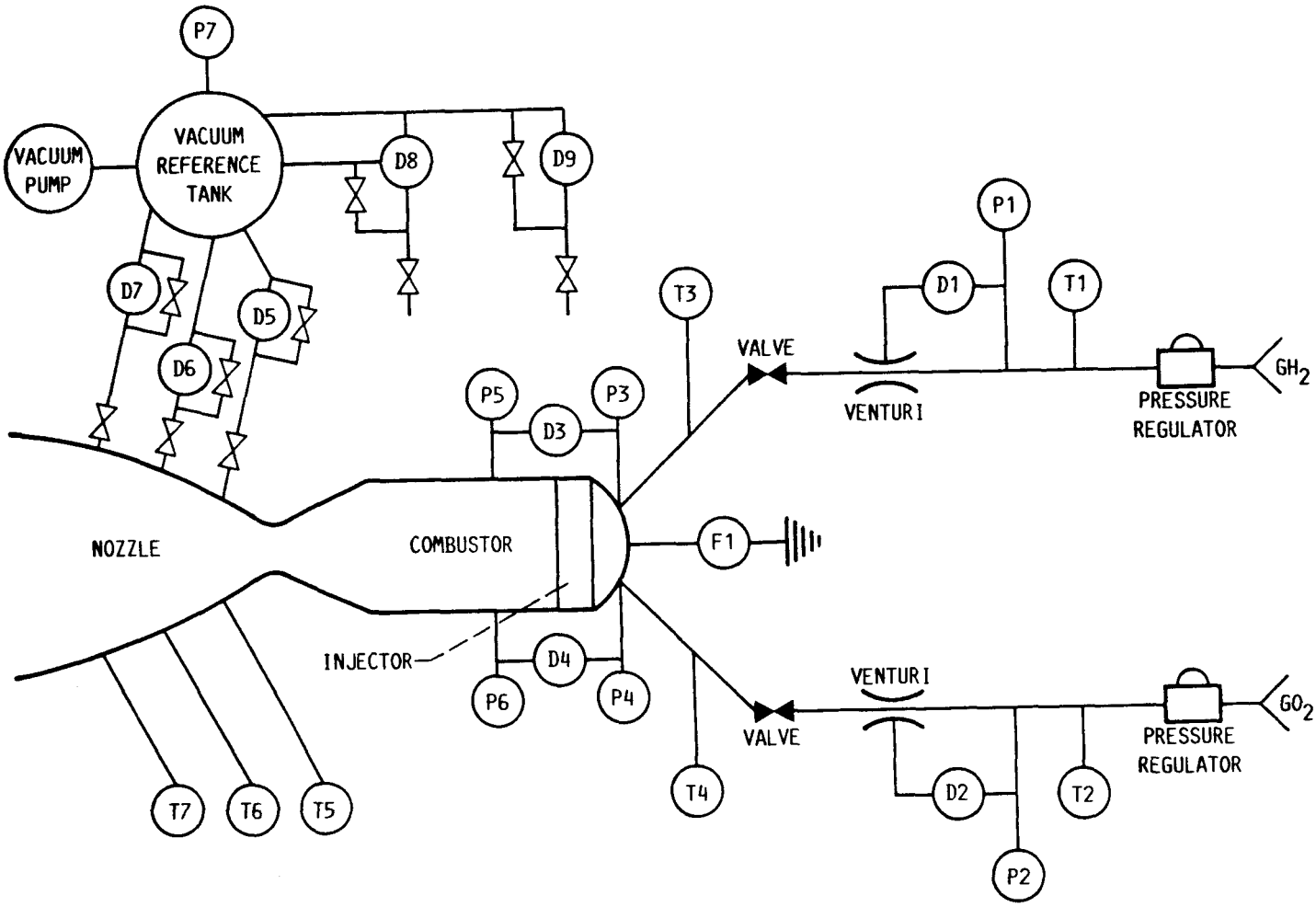

D1	FUEL VENTURI ΔP	D9	ALTITUDE ΔP	P7	VACUUM REFERENCE PRESSURE
D2	OXYGEN VENTURI ΔP	F1	THRUST	T1	FUEL SUPPLY TEMPERATURE
D3	FUEL INJECTION ΔP	P1	FUEL SUPPLY PRESSURE	T2	OXYGEN SUPPLY TEMPERATURE
D4	OXYGEN INJECTION ΔP	P2	OXYGEN SUPPLY PRESSURE	T3	FUEL INJECTION TEMPERATURE
D5	NOZZLE WALL ΔP	P3	FUEL INJECTION PRESSURE	T4	OXYGEN INJECTION TEMPERATURE
D6	NOZZLE WALL ΔP	P4	OXYGEN INJECTION PRESSURE	T5	NOZZLE WALL TEMPERATURE
D7	NOZZLE WALL ΔP	P5	CHAMBER PRESSURE	T6	NOZZLE WALL TEMPERATURE
D8	ALTITUDE ΔP	P6	CHAMBER PRESSURE	T7	NOZZLE WALL TEMPERATURE

FIGURE 1. - ROCKET ENGINE TEST SET-UP AND INSTRUMENTATION SCHEMATIC.

NASA
National Aeronautics and Space Administration

Report Documentation Page

1. Report No.	2. Government Accession No.	3. Recipient's Catalog No.
NASA TM-100203		

4. Title and Subtitle

A Detailed Description of the Uncertainty for High Analysis Area Ratio Rocket Nozzle Tests at the NASA Lewis Research Center

5. Report Date

6. Performing Organization Code

7. Author(s)

Kenneth J. Davidian, Ronald H. Dieck, and Isaac Chuang

8. Performing Organization Report No.

E-3799

10. Work Unit No.

506-42-11

9. Performing Organization Name and Address

National Aeronautics and Space Administration
Lewis Research Center
Cleveland, Ohio 44135-3191

11. Contract or Grant No.

13. Type of Report and Period Covered

Technical Memorandum

12. Sponsoring Agency Name and Address

National Aeronautics and Space Administration
Washington, D.C. 20546-0001

14. Sponsoring Agency Code

15. Supplementary Notes

Prepared for the 24th JANNAF Combustion Meeting, Monterey, California, October 5-9, 1987.
Kenneth J. Davidian, NASA Lewis Research Center; Ronald H. Dieck, Pratt & Whitney, West Palm Beach, Florida; Isaac Chuang, Summer Student at NASA Lewis Research Center from Massachusetts Institute of Technology, Cambridge, Massachusetts.

16. Abstract

A preliminary uncertainty analysis has been performed for the High Area Ratio Rocket Nozzle test program which took place at the altitude test capsule of the Rocket Engine Test Facility at the NASA Lewis Research Center. Results from the study establish the uncertainty of measured and calculated parameters required for the calculation of rocket engine specific impulse. A generalized description of the uncertainty methodology employed is provided. Specific equations used and a detailed description of the analysis are presented. Verification of the uncertainty analysis model was preformed by comparison with results from the experimental program's data reduction code. Final results include an uncertainty for specific impulse of 1.30 percent. Largest contributors to this uncertainty were calibration errors from the test capsule pressure and thrust measurement devices.

17. Key Words (Suggested by Author(s))	18. Distribution Statement
Uncertainty analysis Rocket engine tests Specific impulse	Unclassified - Unlimited Subject Category 20

19. Security Classif. (of this report)	20. Security Classif. (of this page)	21. No of pages	22. Price*
Unclassified	Unclassified	29	A03

NASA FORM 1626 OCT 86

*For sale by the National Technical Information Service, Springfield, Virginia 22161